04

Spatial-spectral filtering of a light field using a phase light modulator

© N.G. Stsepuro, M.S. Kovalev

Lebedev Physical Institute, Russian Academy of Sciences,
119991 Moscow, Russia

e-mail: stsepuro.ng@lebedev.ru

Received December 16, 2022
Revised January 13, 2023
Accepted December 28, 2023

An improved approach to the synthesis of holographic filters, which are achromatic computer-generated Fourier holograms, is demonstrated, taking into account the spatial and spectral characteristics of the light field. An experimental testing of the obtained filters was carried out based on the use of a holographic wavefront sensor operating on the principles of correlation analysis, using several quasi-monochromatic radiation sources. Using the proposed filters, the longitudinal chromatic aberration was measured, the value of which was $\lambda/3$ with an error of $\lambda/50$.

Keywords: spatial filtering, correlation analysis, Fourier holograms, polychromatic radiation.

DOI: 10.61011/EOS.2023.02.55776.17-23

Introduction

Fourier optics — is a continually evolving field of coherent optics in which the application of linear oscillation theory is used to solve problems of spatial structure transformation of light fields or spatial filtering [1]. Science and technology directions addressed by linear spatial filtering techniques include:imaging of phase objects using optical [2] and scanning electron microscopy [3] while implementing a shadow and digital approach; pattern recognition [4–6] based on correlation recognition techniques; synthesis of optical systems with a given light field transformation algorithm [7] by using diffractive optical elements and improving the image quality and performance of optical systems based on frequency field filtering; non-interference methods to extract phase information from intensity distributions, etc. [8–11].

When dealing with wavefields of light beams, their complex amplitude is usually represented as two related components — amplitude and phase distribution. Quantitative imaging of the field phase component, often called wavefront reconstruction or aberration measurement, is usually the most difficult procedure [12]. Today, wavefront detectors (WFSs) [13] are widely used in various areas of physics for complex field amplitude aberration detection tasks. These devices include the well-known Hartmann [14] and Shack-Hartmann (SHS) [15,16] sensors, curvature sensors [17], pyramidal sensors [18], and holographic WFS [19–21]. The operation principle of the presented sensors, with the exception of holographic sensors, is based on the analysis of the intensity distribution of an image or set of images by means of a matrix image sensor (MIS).

In turn, holographic WFSs are based on the principle of transforming the light wave phase into its intensity by spatial filtering of the radiation using different holograms (Fig. 1, *a*). The use of such elements increases the method performance and reduces the holographic sensor sensitivity to amplitude and phase fluctuations. However, as it is known from [22], the diffraction efficiency of such holograms decreases inversely proportional to the squared number of holograms due to limitations of the dynamic range of the recording media. This leads to a significant reduction in the intensity of the waves to be reconstructed for each hologram component. In addition, intermodal (crosstalk) noise is generated during the reconstruction of multiplexed holograms, resulting in a reduction of the signal-to-noise ratio in the analysis plane [23].

This issue can be solved by using a single hologram in combination with spatial filtering and correlation analysis techniques [24]. The essence of the correlation analysis method is to calculate a two-dimensional correlation function between the input and reference distributions of the complex field amplitude [25]. Spatial filters in the form of holograms can act as reference distributions of the complex field amplitude in optical correlators [26]. At the present time, methods for synthesizing these filters allow them to be computed so that they are invariant to displacement, rotation and/or scaling of the input distribution of the complex field amplitude [27].

With the development of computer and digital holography [28] techniques, as well as radiation modulation and registration techniques, the process of synthesizing spatial filters and correlation analysis has become easier. Modern optical correlators are based on spatiotemporal light modulators (SLMs) or digital micro-mirror devices [4] for filter output and matrix image sensor (MIS) for registering the correlation response in the analysis plane [6].

In the present work, a hologram with invariance to wavelength changes of the analyzed radiation is proposed for the analysis of quasi-monochromatic and polychromatic

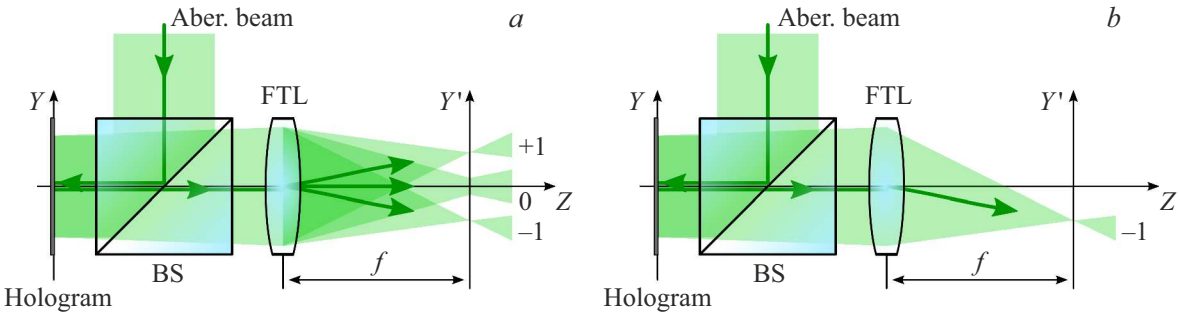

Figure 1. (*a*) Schematic of a holographic DFV [4]. (*b*) Holographic DFV scheme used in the paper

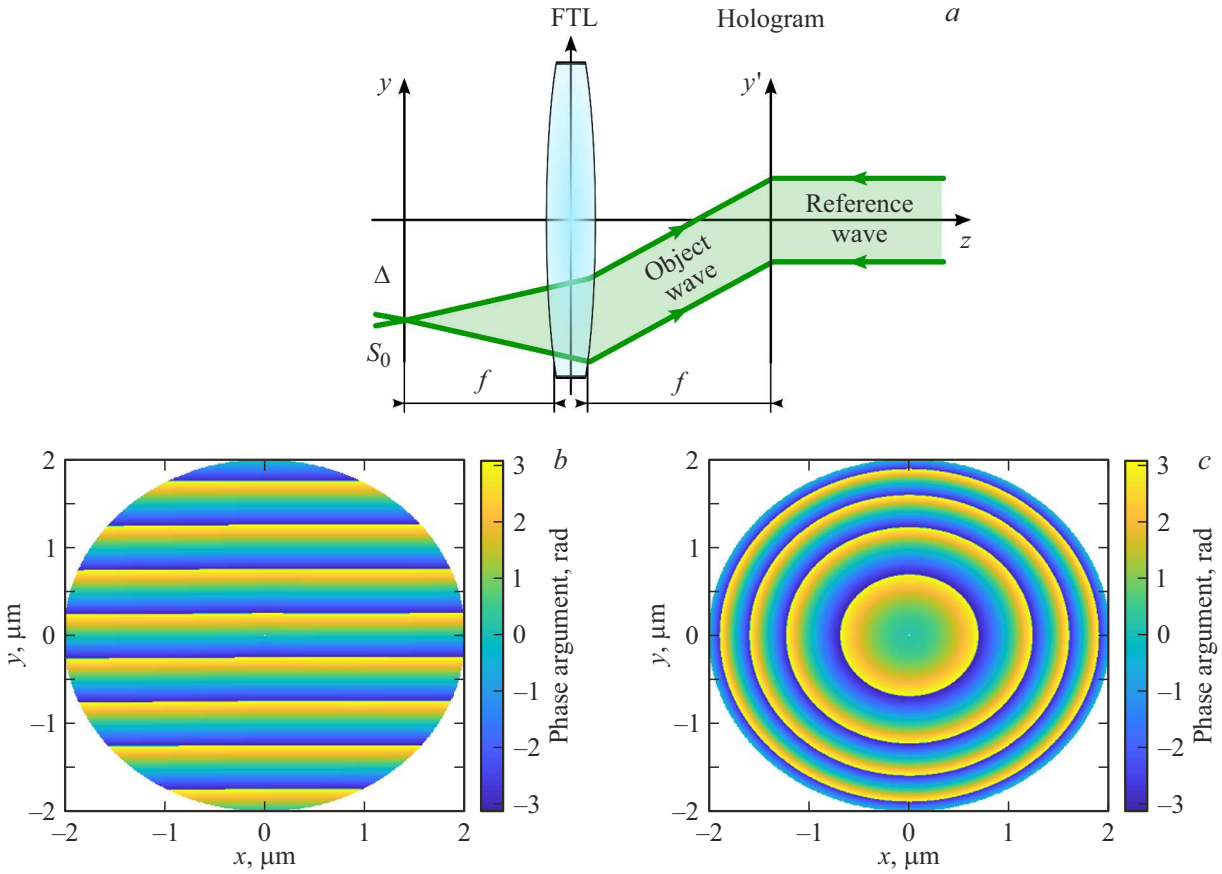

Figure 2. (*a*) Modified version of the van der Lugt hologram synthesis scheme; distributions of the phase argument of the object (*b*) and reference (*c*) waves in the hologram recording plane.

light fields in a holographic WFS. Based on the previously presented implementation scheme of the holographic wavefront sensor (Fig. 1, *b*) [29,30], which operates on the principles of correlation analysis, the synthesized spatial-spectral filters will be tested in the form of computer-generated Fourier holograms (CGHs).

Methods and approaches

Let us consider a mathematical model of the holographic filter synthesis using computer holographic techniques and taking into account the features of the optical scheme [31] shown in Fig. 2, *a*. In this optical scheme, the subject wave is generated by a point quasi-monochromatic radioation source S_0 shifted by Δ relative to the optical axis of the system. In this case, the radiation source is in the front focal plane of the Fourier Transform Lens (FTL), which has a focal length f.

The spherical wave propagating from the radiation source is converted into a plane wave after passing through the FTL. This wave in the formation plane of the holographic filter can be described by the product of the complex spectrum from the radiation source located in the optical

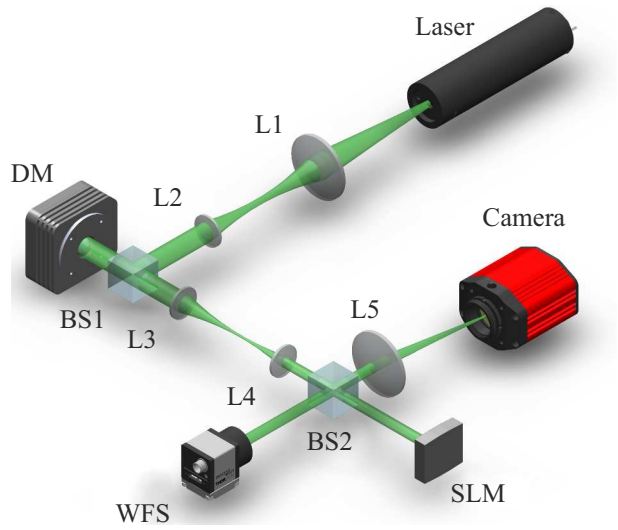

Figure 3. Equivalent optical scheme of the experimental unit. DM — deformable mirror, BS — beam-splitting cube, WFS — wavefront sensor and SLM — spatial light modulator.

axis of the system and the phase shift function [1]

$$\tilde{E}(x', y') \sim \exp\left[-j\frac{2\pi\Delta}{\lambda f}y'\right], \quad (1)$$

where Δ — magnitude of shift relative to the optical axis, λ — wavelength of radiation source, f — focal length of lens [27]. The phase argument distribution in the hologram formation plane will correspond to Fig. 2, *b*.

In this case, the reference wave $R_{ref}(x', y')$ is generated from a quasi-monochromatic radiation source having an intensity value constant across the aperture. In this case, the phase multiplier of the wave represents the following function:

$$R_{ref}(x', y') = \exp\left[j\frac{2\pi}{\lambda}f_{ref}(x', y')\right], \quad (2)$$

where $f_{ref}(x', y')$ — the spatial phase shift caused by the aberration. It can be represented as the sum of orthogonal basis functions

$$f_{ref}(x', y') = \sum_n C_n W_n(x', y'), \quad (3)$$

where C_n — set of weighted coefficients of Zernike polynomials; $W_n(x', y')$ — Zernike polynomials which were first defined in polar coordinates and then converted to Cartesian coordinates using the known methods [32]. Like all other basis functions describing aberrations, the weight coefficients of the Zernike polynomials can be defined in wavelengths and written in the form

$$C_n = N_n\lambda, \quad (4)$$

where N_n — is a real number. Given equations (3) and (4), the reference wave (equation (2)) can be represented by the following analytical expression:

$$R_{ref}(x', y') = \exp\left[j\frac{2\pi}{\lambda}\sum_n N_n\lambda W_n(x', y')\right]. \quad (5)$$

Fig. 2, *c* gives an example of the phase argument distribution of a reference wave for the case where the wavefront can be described by a Zernike polynomial corresponding to a defocusing aberration.

The phase holographic filters used in this paper were derived from mathematical transformations over the complex sum of the reference and object wave functions based on the Jacobi-Anger [1] properties. The result can be represented by an analytical expression of the form:

$$H(x', y') = \exp\left(j2\pi\left[\sum_n N_n W_n(x', y') - \frac{\Delta}{\lambda f}y'\right]\right). \quad (6)$$

Of particular importance in the use of such holograms is the ability to quickly output them using the amplitude or phase modulators that provide full phase modulation from 0 to 2π, with a high fill factor of 93% and a 8 bit address to display halftones [6].

Experiment

The calculated holographic filters were tested on an experimental unit, the equivalent scheme of which is shown in Fig. 3. This optical scheme has been realized using four independent semiconductor laser sources with operating wavelengths of 473, 532, 561 and 659 nm. The radiation source continuously generates quasi-monochromatic radiation, which, as it passes through the Kepler telescope system, falls onto a piezoelectric deformable mirror (DM) of 10 mm diameter. The Kepler system used is achromatic and consists of two lenses L1 and L2, respectively.

In this case, a controlled wavefront (WF) shape is given by the DM by introducing a geometric phase shift in the reflection of the incident beam on the mirror as a result of its deformation. The WF shape is detected by means of a Shack-Hartmann Sensor (SHS), which operates with the DM in „feedback mode“. The „feedback mode“ is realized by optically pairing the apertures of DM and SHS using the Kepler achromatic telescope system (L3 and L4) with magnification $3^{\times}$.

As a result of radiation diffraction from the holographic filters output on the SLM, a single main diffraction maximum is formed in the rear focal plane of the achromatic FTL, which is detected by the matrix image senso (MIS).

Discussion of experimental results

Using the example of quasi-monochromatic radiation whose wavelength is 659 nm as an example, consider the basic properties of a Fourier CGH. Using DM, the WF shape was so distorted that its surface could only be

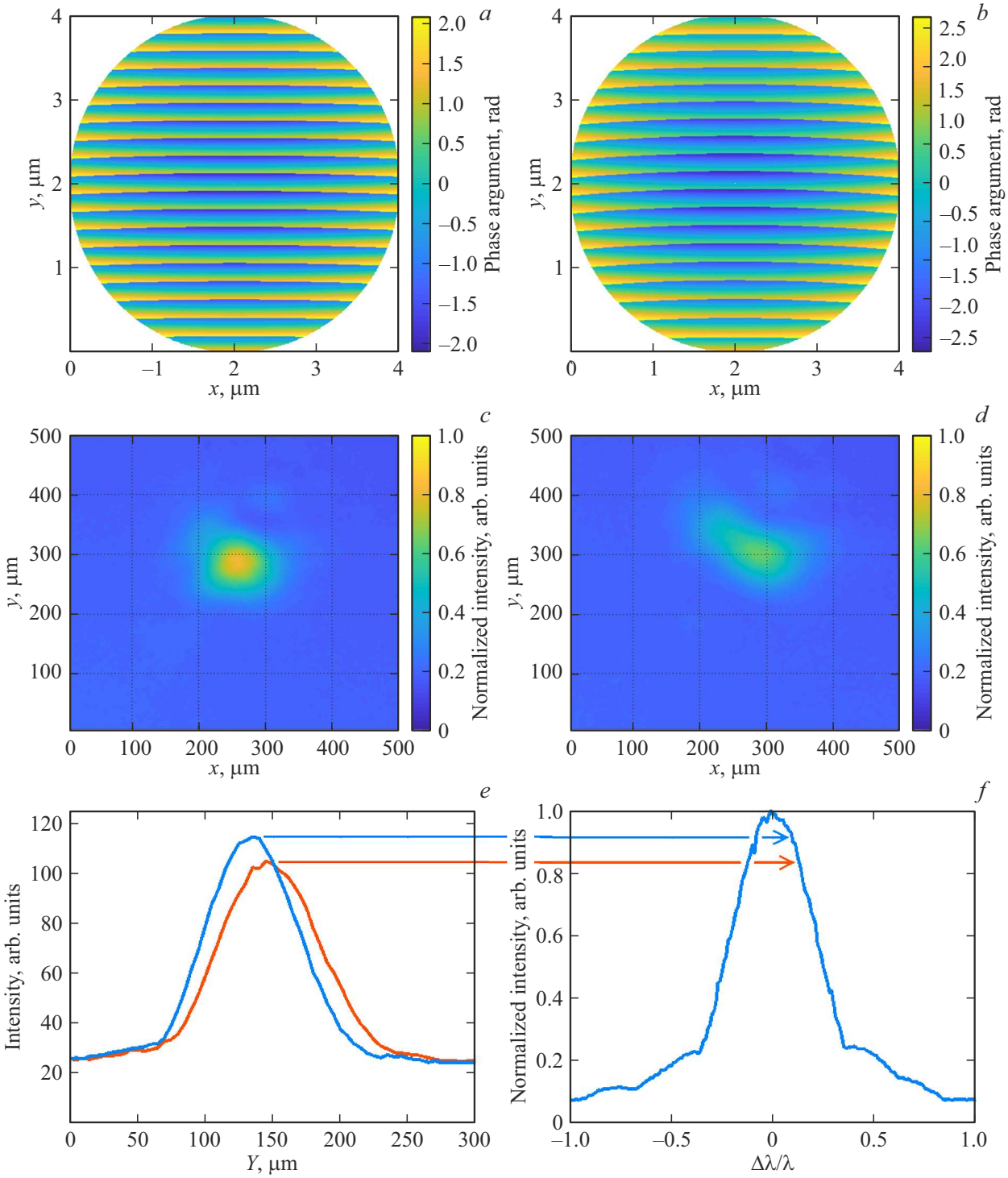

Figure 4. $(a), (b)$ Example holograms used; $(c), (d)$ an example of the intensity distributions recorded, (e) their cross sections and (f) the normalized amplitude of the correlation function maxima.

described by a single Zernike polynomial. In general case, holographic filters with different values of weight coefficients of Zernike polynomials were outputted iteratively on the SLM with a step of 0.01λ. As a result, the intensity distribution in the back focal plane of the FTL changed. Fig. 4, *a, b* shows the phase argument distributions of the holographic filter with a Zernike polynomial weighting factor value of 0.2λ and 0.1λ, respectively, and Fig. 4, *c, d* shows the 2D intensity distribution in the MIS setup plane when the filter outputs from Fig. 4, *a, b*.

From each resulting two-dimensional intensity distribution, the maximum value (Fig. 4,*f*) was taken, and the

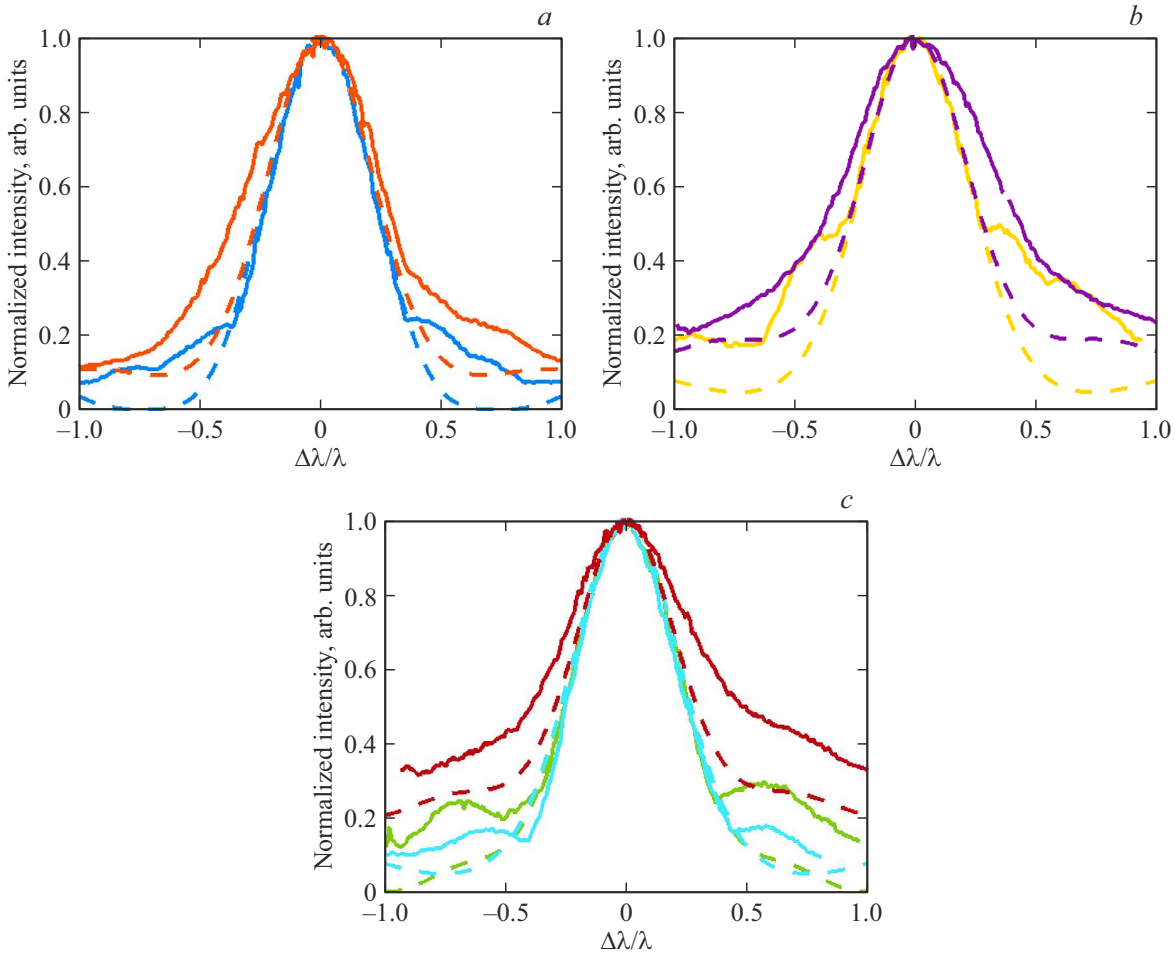

Figure 5. Dependence of the CF peak amplitude on the value of the weight coefficient of the Zernike polynomial for the corresponding WF aberration: (*a*) 2nd radial order; (*b*) 3rd radial order; (*c*) 4th radial order; The dashed lines indicate the results of the numerical study, the solid lines — the results of the experimental study.

dependence of the maximum intensity value on the value of the Zernike polynomial coefficient for a particular aberration in the holographic filter was constructed from them. Hence, there is a one-to-one relationship between them, and this relationship corresponds to the normalized amplitude of the correlation function (CF) maxima (Fig. 4, *e*).

According to the above algorithm, the first 15 Zernike polynomials describing WF aberrations and different values of the weight coefficients were plotted. Fig. 5 shows the results of numerical and experimental studies for various Zernike polynomials describing in Fig. 5,*a* 2nd radial order aberrations (defocusing (blue lines), astigmatism under 0° (orange lines) in Fig. 5, *b* — 3rd radial order aberrations (3rd order Y coma (purple lines), trefoil (yellow lines), and in Fig. 5, *c* - 4th radial order aberrations (spherical aberration (blue lines), secondary astigmatism (green lines), trefoil (red lines)) with weighting factor-1λ. It can be seen from the figure that in most cases, there is complete or partial agreement between the profiles of the experimental results and the numerical ones, and the profile of the obtained dependencies indicates the solution uniqueness.

Then, the WF distortions that are described by two or more Zernike polynomials were measured. In this case, forming the dependence of the CF peak amplitude on the value of the weight coefficient of the Zernike polynomial was not changed. However, a specific feature of such field analysis is that the spatial dimension of the resulting dependence depends directly on the number of detected aberrations. Fig. 6 shows in the left column the obtained 2D distributions of the CF peak amplitude, and in the right column - the reconstructed phase distributions in the analyzed beam diameter 4 mm.

Fig. 7 shows cross-sections of the two-dimensional distributions of the CF peak amplitude along the X and Y axis presented in Fig. 6. The analysis of the resulting distributions shows that the type of dependence of the CF peak amplitude for a particular aberration did not change in the presence of other WF distortions. This fact suggests that the spatial filtering-based method does not affect the orthogonal properties of the Zernike polynomials used. The presence of a global maximum of the functions indicates that the solution singularity is preserved.

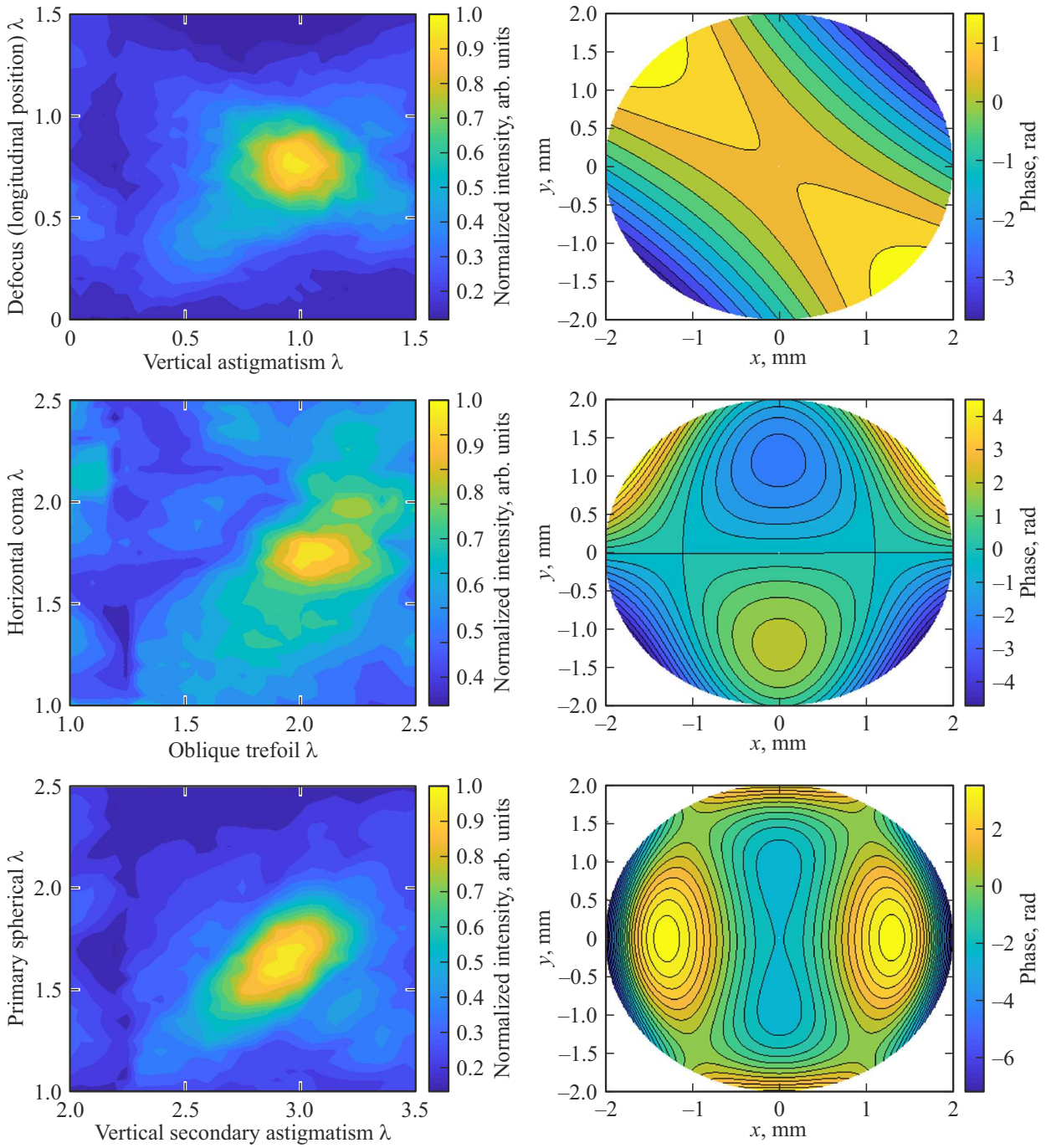

Figure 6. View of two-dimensional distributions of the maximum CF amplitude for the corresponding WF aberrations and reconstructed phase distributions in the analyzed beam.

After analyzing the quasi-monochromatic WF and determining the mutual-ambiguous correspondences, the achromatic properties of the synthesized spatial filters were investigated. For this purpose, a polychromatic WF of three independent coherent quasi-monochromatic radiations with operating wavelengths of 473, 532 and 561 nm was created. Due to the fact that different radiation wavelengths were incident on the DM, the geometric phase shift was different for each wavelength. As a result, in the SLM plane, the WF shape for each wavelength was the same, and the values of the weight coefficient of the Zernike polynomial were different.

As a consequence, 3 main diffraction maxima were observed in the MIS plane, each corresponding to a different wavelength of radiation. The spatial position of the main diffraction maxima was determined by the position of the point source of radiation relative to the optical axis, as well as the wavelength of the radiation incident on the

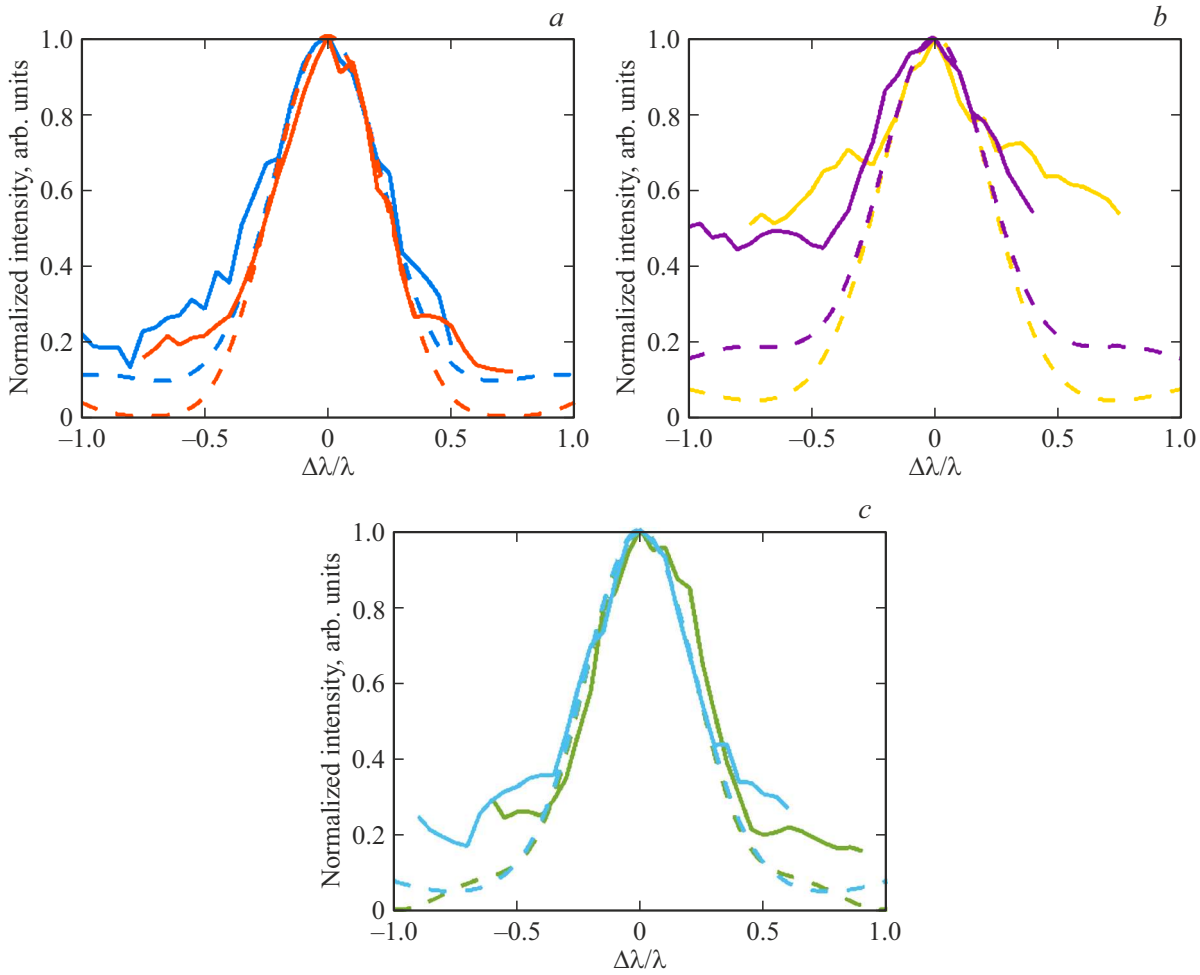

Figure 7. View of cross sections through the global maximum of the two-dimensional maximum CF amplitude dependence for the respective aberrations: (*a*) 2nd radial order; (*b*) 3rd radial order; (*c*) 4th radial order.

hologram when it was reduced. It is worth pointing out the fact that in this case, the holographic filters displayed on the SLM were not modified due to their achromaticity.

Fig. 8 in the left column shows two-dimensional intensity distributions in the plane of the MIS installation, in which, the main diffraction maxima are clearly visible. As before, the intensity of the intensity distribution in the focal plane varies depending on the holographic filters output from the SLM. Fig. 8 shows the cases where the weight coefficient of the Zernike polynomial in the hologram was 0.23λ, 0.43λ and 0.5λ, respectively.

The normalized amplitude of the correlation function maxima was plotted over a range of changing Zernike polynomial weights from 0.1 to 0.6λ at a pitch of 0.01λ. In this case, the one-dimensional dependence has three local maxima, each corresponding to a different radiation wavelength and a different magnitude of WF distortion in the beam under study. This can be clearly seen in Fig. 9, which shows the dependence obtained in this experiment.

If we measure the distance between the local maxima corresponding to the 473 and 561 wavelengths, we can determine the chromatic aberration of the complex field amplitude, which in this case is $\sim \lambda/3$ with respect to the central wavelength of 532 nm.

Conclusion

In the present work, an improved approach to the synthesis of holographic filters, which are achromatic computer-generated Fourier holograms, has been demonstrated. These holograms can be used in various optical matched filtering and correlation analysis techniques. The advantage of using such holograms is that only one correlation response is generated in the correlation analysis plane. This allows increasing the signal-to-noise ratio, decreasing the aperture of the analyzed MIS area, resulting in increasing the method performance; and using the synthesized filters when working with polychromatic radiation due to their invariant properties to changes in the radiation wavelength.

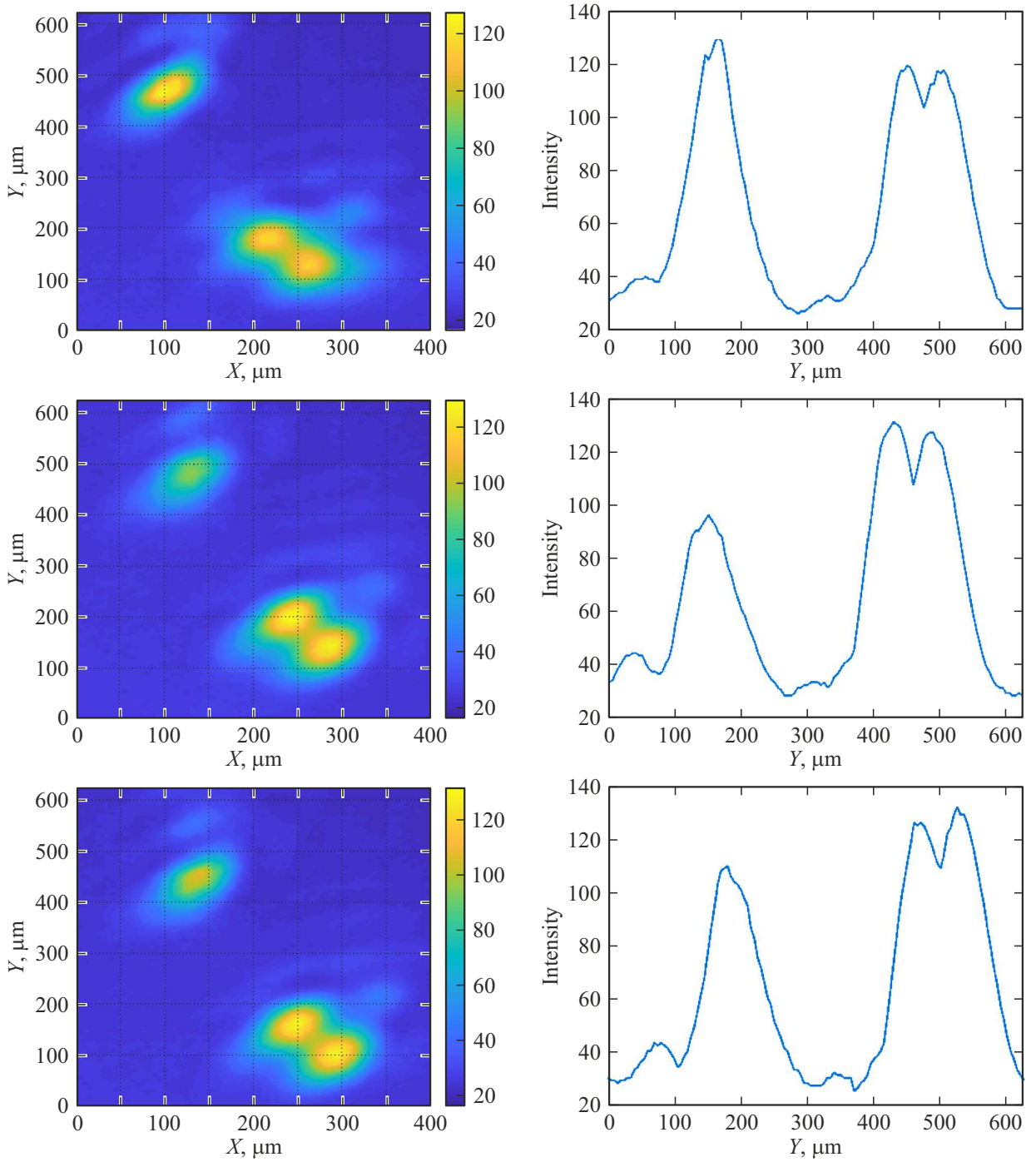

Figure 8. Intensity distribution in the MIS unit plane and their cross-section along the Y-axis for different values of the weight coefficients of the Zernike polynomial.

The method disadvantages include the fact that the filter synthesis scheme used involves the use of a quasi-monochromatic radiation. As a result, the correlation responses generated in the analysis plane are representations of the scattering function of a point of this radiation source. Therefore, in the case of simultaneous operation with several quasi-monochromatic radiation sources, it is essential that the spatial characteristics of the radiation are the same. In the case of a broad-spectrum radiation source (e. g. supercontinuum), there are no such limitations.

Funding

The authors are grateful to the Russian Science Foundation for the financial support of these research within project 21-79-30063.

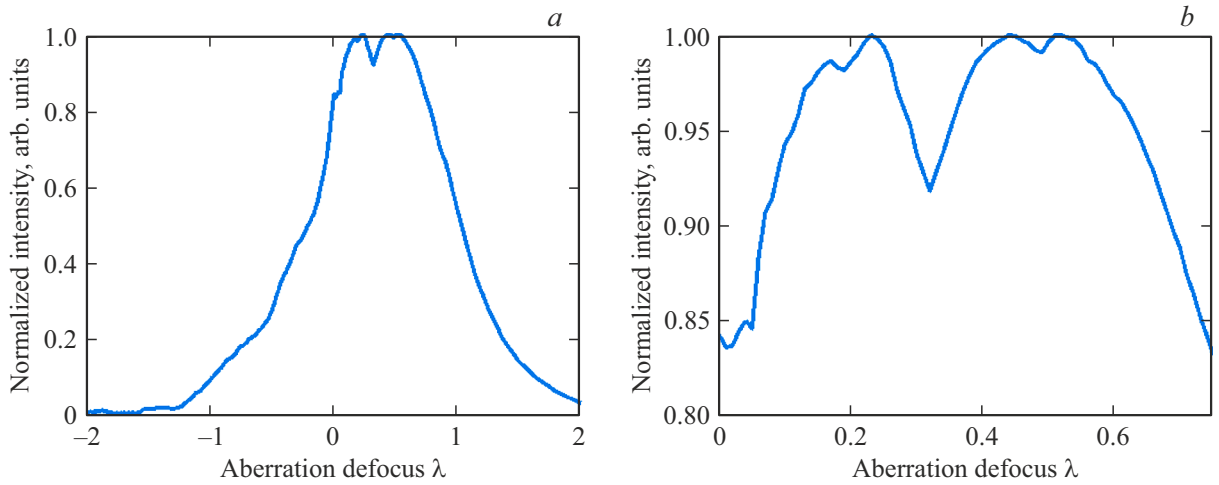

Figure 9. (*a*) Dependence of the CF peak amplitude when detecting polychromatic aberrations; (*b*) enlarged peak amplitude dependence area of CF.

Conflict of interest

The authors declare that they have no conflict of interest.

References

[1] J.W. Goodman. *Introduction to Fourier Optics*, 4th ed. (W.H. Freeman Press, 2017).

[2] Y. Park, C. Depeursinge, G. Popescu. Nat. Photon., **12**, 578B–589 (2018). DOI: 10.1038/s41566-018-0253-x

[3] N. Stsepuro, M. Kovalev, G. Krasin, I. Podlesnykh, Y. Gulina, S. Kudryashov. Photonics, **9**, 815 (2022). DOI: 10.3390/photonics9110815

[4] N. Stsepuro, M. Kovalev, E. Zlokazov, S. Kudryashov. Photonics, **9**, 909 (2022). DOI: 10.3390/photonics9120909

[5] P.A. Cheremkhin, V.V. Krasnov, D.Y. Molodtsov, V.G. Rodin. Opt. Commun., **421**, 73–78 (2018). DOI: 10.1016/j.optcom.2018.03.085

[6] E.Y. Zlokazov. Quantum Electron., **50**, 643 (2020). DOI: 10.1070/QEL17291

[7] N.L. Kazanskiy, S.N. Khonina, S.V. Karpeev, A.P. Porfirev. Quantum Electron., **50** (7), 629 (2020). DOI: 10.1070/QEL17276

[8] I.V. Gritsenko, M.S. Kovalev, N.G. Stsepuro, Y.S. Gulina, G.K. Krasin, S.A. Gonchukov, S.I. Kudryashov. Laser Phys. Lett., **19**, 076201 (2022). DOI: 10.1088/1612-202X/ac7136

[9] B.C. Platt, R. Shack. J. Refract. Surg., **17** (5), 573–577 (2001). DOI: 10.3928/1081-597X-20010901-13

[10] R.R. McLeod, K.H. Wagner. Adv. Opt. Photonics, **6**, 368–412 (2014). DOI: 10.1364/AOP.6.000368

[11] H. Guerboukha, K. Nallappan, M. Skorobogatiy. Adv. Opt. Photonics, **10** (4), 843–938 (2018). DOI: 10.1364/AOP.10.000843

[12] L.G. Ellerbroek. Appl. Opt., **45**, 6568–6576 (2006). DOI: 10.1364/AO.45.006568

[13] J.M. Geary. *Introduction to Wavefront Sensors*, 1st ed. (Bellingham, WA, 1995).

[14] A.G. Poleshchuk, A.G. Sedukhin, V.I. Trunov, V.G. Maksimov. Comput. Opt., **38**, 695–703 (2014). DOI: 10.18287/0134-2452-2014-38-4-695-703

[15] B.C. Platt, R. Shack. J. Refract. Surg., **17**, S573 (2001). DOI: 10.3928/1081-597X-20010901-13

[16] J. Primot. Opt. Commun., **222**, 81–92 (2003). DOI: 10.1016/S0030-4018(03)01565-7

[17] F. Roddier. Appl. Opt., **27**, 1223–1225 (1988). DOI: 10.1364/AO.27.001223

[18] R. Ragazzoni, E. Diolaiti, E. Vernet. Opt. Commun., **208**, 51–60 (2002). DOI: 10.1016/S0030-4018(02)01580-8

[19] M.A.A. Neil, M.J. Booth, T. Wilson. J. Opt. Soc. Am. A, **17**, 1098–1107 (2000). DOI: 10.1364/JOSAA.17.001098

[20] S.N. Khonina, S.V. Karpeev, A.P. Porfirev. Sensors, **20**, 3850 (2020). DOI: 10.3390/s20143850

[21] V.Yu. Venediktov, A.V. Gorelaya, G.K. Krasin, S.B. Odinokov, A.A. Sevryugin, E.V. Shalymov. Quantum Electron., **50**, 614 (2020). DOI: 10.1070/QEL17288

[22] R.J. Collier, C.B. Burckhardt, L.H. Lin. *Optical Holography* (Academic, NY., 1971).

[23] M.A.A. Neil, M.J. Booth, T. Wilson. Opt. Lett., **25**, 1083–1085 (2000). DOI: 10.1364/OL.25.001083

[24] B.V.K.V. Kumar, A. Mahalanobis, R.D. Juday. *Correlation Pattern Recognition* (Cambridge University Press, Cambridge, 2005).

[25] A. Mahalanobis, B.V.K.V. Kumar, S. Song, S.R.F. Sims, J.F. Epperson. Appl. Opt., **33**, 3751–3759 (1994). DOI: 10.1364/AO.33.003751

[26] B.V.K.V. Kumar. Appl. Opt., **31**, 4773–4801 (1992). DOI: 10.1364/AO.31.004773

[27] B. F. Fedorov, R. I. Elman. *Tsifrovaya golografiya* (Nauka, M., 1976). (In Russian).

[28] J.T. Sheridan, R.K. Kostuk, A.F. Gil. J. Opt., **22**, 123002 (2020). DOI: 10.1088/2040-8986/abb3a4

[29] G. Krasin, M. Kovalev, N. Stsepuro, P. Ruchka, S. Odinokov. Sensors, **20**, 4310 (2020). DOI: 10.3390/s20154310

[30] P.A. Ruchka, N.M. Verenikina, I.V. Gritsenko, E.Y. Zlokazov, M.S. Kovalev, G.K. Krasin, S.B. Odinokov, N.G. Stsepuro. Opt. Spectrosc., **127**, 618–624 (2019). DOI: 10.1134/S0030400X19100230

[31] V.V. Orlov, V.Yu. Venediktov, A.V. Gorelaya, E.V. Shubenkova, D.Z. Zhamalatdinov. Opt. Laser Technol., **116**, 214–218 (2019). DOI: 10.1016/j.optlastec.2019.03.028

[32] V. Lakshminarayanan, A. Fleck. J. Mod. Opt., **58**, 545–561 (2011). DOI: 10.1080/09500340.2011.633763

Translated by Y.Deineka